

# Soft Plaque Detection and Automatic Vessel Segmentation

Shawn Lankton<sup>1</sup>, Arthur Stillman<sup>2</sup>, Paolo Raggi<sup>2</sup>, and Allen Tannenbaum<sup>1,2</sup>

<sup>1</sup> Georgia Institute of Technology, Atlanta, GA, USA

<sup>2</sup> Emory University School of Medicine, Atlanta, GA, USA

**Abstract.** The ability to detect and measure non-calcified plaques (also known as *soft plaques*) may improve physicians' ability to predict cardiac events. This is a particularly challenging problem in computed tomography angiography (CTA) imagery because plaques may have similar appearance to nearby blood and muscle tissue. This paper presents an effective technique for automatically detecting soft plaques in CTA imagery using active contours driven by spatially localized probabilistic models. The proposed method identifies plaques that exist within the vessel wall by simultaneously segmenting the vessel from the inside-out and the outside-in using carefully chosen localized energies that allow the complex appearances of plaques and vessels to be modeled with simple statistics. This method is shown to be an effective way to detect the minute variations that distinguish plaques from healthy tissue. Experiments demonstrating the effectiveness of the algorithm are performed on eight datasets, and results are compared with detections provided by an expert cardiologist.

## 1 Introduction

Heart disease remains the leading cause of death in western countries. A number of recent studies have demonstrated that the presence of vascular plaques can be a significant indicator of risk for cardiac events [1]. The advent of multi-detector computed tomography (MDCT) and computed tomography angiography (CTA) allows one to non-invasively image these plaques, which can be categorized as either *calcified* or *non-calcified* based on their composition. Calcified plaques are easily discernible due to their high density and corresponding bright appearance in computed tomography (CT)

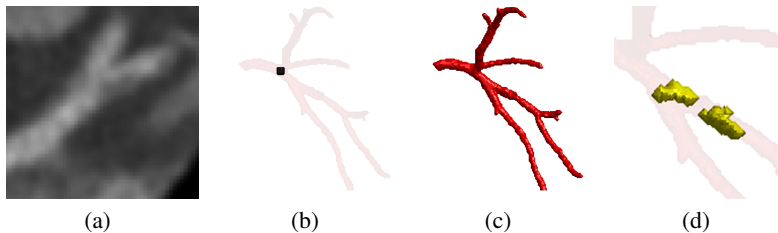


**Fig. 1.** Using CTA Imagery shown in (a) and a single-point initialization shown as the dark spot in (b), the vessel is segmented (c) and used to detect non-calcified plaques (d) in the vessel tree.

imagery. Consequently, several techniques have been presented to automatically detect calcified plaques with reasonable accuracy [2, 3]. Alternatively, non-calcified plaques, also known as *soft plaques*, have a CT attenuation similar to blood and myocardial tissue making them difficult to detect, even for trained experts [4, 5]. Detection and segmentation of soft plaques is essential given that non-calcified plaques are much more likely than calcified plaques to rupture and cause a variety of acute coronary syndromes [6].

This paper presents an effective and straightforward technique for automatically detecting soft plaques in CTA imagery based on multiple segmentations of the vessel wall. The segmentations are performed using multiple active contours driven by spatially localized statistical models that allow the complex appearances of plaques and vessels to be described with simple statistics. First, the vessel tree is extracted using a single, user-provided initialization point. Next two surfaces are constructed that lie just inside and just outside the vessel wall. An active contour model driven by a localized energy designed for plaque detection is then employed to simultaneously segment the interior and exterior of the vessel wall. Finally, areas where these two segmentations do not match are identified as potential regions of non-calcified plaque. Figure 1 shows an example of the imagery used, the initialization, the segmented vessel, and the detected plaque.

To the best of our knowledge, there is little published literature on automatic soft plaque detection in CTA imagery. The one recent paper to explicitly address this problem by Renard and Yang [7] also utilizes localized information to segment the interior and exterior of the vessel wall. The method in [7] requires pre- and post processing of the volume, describes no way to detect plaques in branching vessels, and uses an adaptive thresholding scheme for segmentation. By contrast, the present work casts the problem in a variational active contour framework that operates directly on the raw imagery thus reducing algorithmic complexity and the number of parameters. Furthermore, the proposed method naturally handles branching vessels and benefits from the geometric properties of active contours.

The segmentation and detection algorithms are described in detail in Section 2. In Section 3, experiments are shown on several vessel trees including the right coronary artery (RCA), left circumflex (LCX), and left anterior descending (LAD). The results are then compared with detections made by an expert cardiologist to validate the method. Finally, conclusions and directions for future work are given in Section 4.

## 2 Detection Algorithm

In this section, the framework used to guide an active contour segmentation with localized statistics is summarized, and two separate energies are shown. The behaviors and underlying assumptions are described in detail for each of these energies, which are used for vessel segmentation and plaque detection, respectively. Additionally, the process for vessel segmentation, creation of the interior and exterior initialization surfaces, and soft plaque detection are discussed.

## 2.1 Localized Contours

The detection method presented in this paper makes extensive use of localized active contours as described recently by several authors [8–10]. This technique allows region-based segmentation energies to be spatially localized such that statistical models of the foreground and background adapt to image information as it changes over the domain of the image. This allows for improved modeling accuracy with simplified statistical models. Furthermore, it is particularly powerful for segmenting vessels, which often exhibit changing image intensities over their length, and for the identification of non-calcified plaques, which typically have only slight intensity differences from surrounding structures.

To define these localized active contours, assume that the domain  $\Omega \subset \mathbb{R}^n$  of a given intensity image  $I$  is partitioned into regions by an evolving surface in 3D or contour  $C$  in 2D, where  $C$  is embedded in a signed distance function  $\phi : \mathbb{R}^n \rightarrow \mathbb{R}$  such that  $C = \{x | \phi(x) = 0\}$  [11, 12]. The interior region is defined by the Heaviside function,  $\mathcal{H}\phi$ , which is 1 when  $\phi < 0$ , 0 when  $\phi > 0$ , and has a smooth transition through 0. Similarly, the interface at the zero level set can be denoted by  $\delta\phi$ , the derivative of  $\mathcal{H}\phi$ , which is 1 when  $\phi = 0$  and 0 far from the interface. Localized active contours also utilize a characteristic function,  $\mathcal{B}(x, y)$  representing a ball of radius  $r$  centered at  $x$  such that  $\mathcal{B}(x, y) = 1$  when  $\|x - y\| \leq r$ . Given these definitions localized active contours minimize energy functionals of the form

$$E(\phi) = \int_{\Omega_x} \delta\phi(x) \int_{\Omega_y} \mathcal{B}(x, y) \cdot F(I, \phi, x, y) dy + \lambda \delta\phi(x) |\nabla\phi(x)| dx, \quad (1)$$

where  $\lambda$  is a scalar weight on the arc-length and  $F(I, \phi, x, y)$  represents an internal energy functional that is selected based on the application. The sparse level set representation presented by Whitaker in [13] is used for implementation due to its accuracy and speed.

To segment the vessels, an internal energy based on the one presented by Chan and Vese in [14] is used while a separate energy, similar to the one proposed by Yezzi *et al.* in [15], is used for detection of plaques. Both internal energies make use of localized interior and exterior means

$$\mu_{\text{in}}(x) = \frac{\int_{\Omega_y} \mathcal{B}(x, y) \cdot \mathcal{H}\phi(y) \cdot I(y) dy}{\int_{\Omega_y} \mathcal{B}(x, y) \cdot \mathcal{H}\phi(y) dy} \quad (2)$$

$$\mu_{\text{out}}(x) = \frac{\int_{\Omega_y} \mathcal{B}(x, y) \cdot (1 - \mathcal{H}\phi(y)) \cdot I(y) dy}{\int_{\Omega_y} \mathcal{B}(x, y) \cdot (1 - \mathcal{H}\phi(y)) dy}, \quad (3)$$

which measure local regions centered around a point  $x$  as shown in Figure 2.

More specifically, for vessel segmentation, the *uniform modeling* energy, based on [14] is employed. With this choice of internal energy, Equation (1) is minimized when local interior and exterior regions are well characterized by  $\mu_{\text{in}}(x)$  and  $\mu_{\text{out}}(x)$ , respectively. Hence, the interior energy for uniform modeling is given by

$$F_{\text{UM}} = \mathcal{H}\phi(y) (I(y) - \mu_{\text{in}}(x))^2 + (1 - \mathcal{H}\phi(y)) (I(y) - \mu_{\text{out}}(x))^2. \quad (4)$$

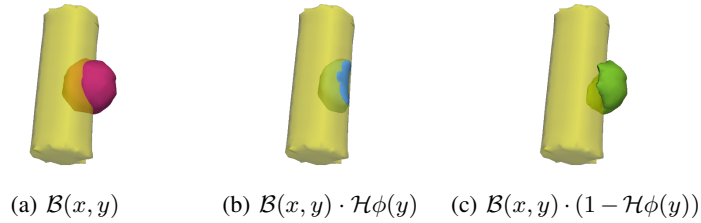


**Fig. 2.** Visualization of the local regions over which statistics are computed. The cylinder represents the surface  $C$ . The dark ball in (a) shows the full ball selected by  $\mathcal{B}(x, y)$  while dark regions in (b) and (c) show the local interior and exterior regions respectively.

This energy is ideal for vessel segmentation, because it allows the surface to expand into areas of similar local intensity as long as a larger difference exists between local interiors and exteriors. This allows rapid segmentation of vessels despite changing intensities along the length of the vessel.

For soft plaque detection, the *means separation* interior energy is utilized. This energy is based on an energy presented in [15] and is minimized when the difference between  $\mu_{\text{in}}(x)$  and  $\mu_{\text{out}}(x)$  is maximized. Thus, the internal energy can be expressed as

$$F_{\text{MS}} = -(\mu_{\text{out}}(x) - \mu_{\text{in}}(x))^2. \quad (5)$$

This is ideally suited for detection, because expansion into nearby regions that have slightly different intensities is discouraged, even if the local means are similar. This more stringent constraint is quite valuable when attempting to differentiate between vascular plaques and surrounding tissue.

## 2.2 Vessel Segmentation

The first step in detecting soft plaques is to segment a given vessel tree by minimizing Equation (1) with the uniform modeling internal energy from Equation (4). This energy is particularly powerful for segmenting vessels. By looking locally, it is able to accommodate variations in intensities that occur over the length of vessels, while also remaining sensitive to slight intensity differences that separate vessels from adjacent structures. Hence, the entire vessel can be captured from a single-point initialization while at the same time preventing leaks into nearby contrast-filled heart chambers. In the event that the vessel is completely occluded, additional initialization points may be required to achieve a full segmentation. This localized active contour approach also responds naturally to branches in the vessel, capturing them automatically without any special schemes to detect their presence.

During vessel extraction and plaque detection, a restricted domain  $\tilde{\Omega}$  is used, which only includes voxels representing the heart and ignores very dark voxels representing air present in the lungs. This restricted domain is created by excluding from  $\Omega$  any points that fall below a threshold of -600 Hounsfield units (HU). This threshold is significantly below the ranges for blood, plaques, and myocardial tissues in all CTA

data. Using a single-point initialization within the vessel, the entire vessel structure can be extracted by updating  $\phi$  according to.

$$\begin{aligned} \frac{d\phi(x)}{dt} = & \delta\phi(x) \int_{\tilde{\Omega}_y} \mathcal{B}(x, y) \cdot \delta\phi(y) \cdot \left( (I(y) - \mu_{\text{in}}(x))^2 - (I(y) - \mu_{\text{out}}(x))^2 \right) dy \\ & + \lambda \text{div} \left( \frac{\nabla\phi(x)}{|\nabla\phi(x)|} \right) |\nabla\phi(x)|. \end{aligned} \quad (6)$$

The parameter values  $\lambda = 0.1 \max(|\frac{d\phi}{dt}|)$  and  $r = 5$  mm are used throughout. This choice for  $r$  is reasonable, representing the maximum possible diameter for vessels in the vessel tree. Figure 3 shows the initializations, and resulting vessel segmentations on the LAD, LCX and RCA vessel trees.

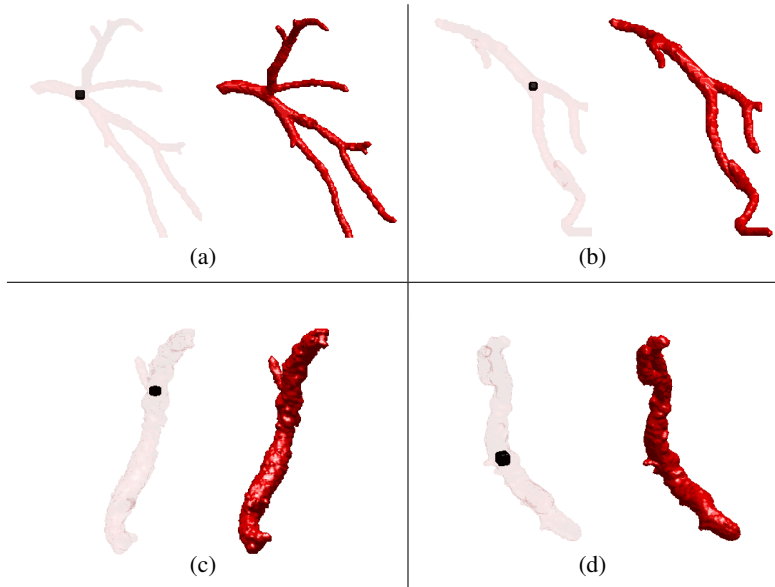


**Fig. 3.** 3D Renderings of initializations and segmentation results on the (a) LAD, (b) LCX, and (c, d) RCA. For each, the initialization is shown on left as a dark point and the resulting segmentation is shown on the right.

### 2.3 Constructing the Initialization

Using the vessel segmentation as starting point, two surfaces are created that act as initializations for the detection step. These initializations are formed inside and outside of the initial vessel segmentation so that plaques, which form within the vessel wall, will be located between the two surfaces.

To create the interior surface a third localized energy is employed that relies only upon the geometry of the surface and not image information. Here, the internal energy

defined as  $F_{\text{SHRINK}} = \mathcal{H}\phi(y)$  penalizes interior area locally. Thus as the energy is minimized, the segmented vessel surface will thin with each iteration, but the thickest parts of the vessel surface will thin the fastest. Thus by running a few iterations, an interior surface is created that preserves the topology of the original surface and is always inside of it. This is similar to a medial axis (skeleton) except that relative thicknesses of vessel segments are preserved, meaning that although all segments become thinner, thick segments remain thicker than thin segments. Also, the surface resulting from this process will have a definite interior so that image statistics can be computed within it.

The exterior initialization is created by evolving the segmented vessel surface outward along its unit normal for several iterations. In our case, this is functionally equivalent to morphological dilation with a  $5 \text{ mm} \times 5 \text{ mm}$  ball-shaped structuring element. The end result is a surface which is always outside of the initial vessel segmentation.

## 2.4 Plaque Detection

The next step involves the application of the means separation internal energy from Equation (5) to pull the two initial surfaces towards each other. Where no soft plaque exists, the two surfaces will meet on the vessel wall. However, if a soft plaque deposit exists between the two evolving surfaces they will each stop on the plaque boundary and remain separated from one another. By identifying areas where the two contours do not meet, soft plaques are detected.

The interior and exterior surfaces created in Section 2.3, are each deformed to minimize the means separation energy using the update function

$$\begin{aligned} \frac{d\phi(x)}{dt} = & \int_{\tilde{\Omega}_y} \mathcal{B}(x, y) \cdot \delta\phi(y) \left( \frac{(I(y) - \mu_{\text{out}}(x))^2}{A_{\text{out}}(x)} - \frac{(I(y) - \mu_{\text{in}}(x))^2}{A_{\text{in}}(x)} \right) dy \\ & + \lambda \text{div} \left( \frac{\nabla\phi(x)}{|\nabla\phi(x)|} \right) |\nabla\phi(x)| \end{aligned} \quad (7)$$

where  $A_{\text{in}}(x)$  and  $A_{\text{out}}(x)$  are defined as the areas of the local interior and exterior regions, respectively. Minimizing this energy deforms the surface such that local means are pulled apart as much as possible.

Initially, the local interior regions of the inner surface will only include bright blood voxels. As the surface deforms, it will expand to capture more voxels containing blood but will not expand into slightly darker soft plaque voxels. Similarly, the exterior surface will not contract if doing so would cause soft plaque voxels, which are slightly brighter than myocardium voxels, to move into its local exterior regions. This behavior allows the two evolving surfaces to capture soft plaques between each other because neither will move into the plaque voxels when driven by the localized means separation energy.

The two surfaces are evolved until convergence, and soft plaques are defined as areas where the distance between the two surfaces is larger than one voxel. A label map  $P$ , which is 1 where plaques exist and 0 elsewhere, is defined as

$$P = (1 - \mathcal{H}(\phi_{\text{interior}})) \cdot \mathcal{H}(\phi_{\text{exterior}} + 1). \quad (8)$$

### 3 Experiments

The results of experiments on MDCT scans of 8 patients undergoing CTA, for which we were able to obtain expert markings of soft plaques, are presented in this section. All scans were taken with a Siemens Sensation 64-slice multi detector CT machine and examined by an expert investigator to mark soft plaque deposits. For each dataset, plaques were detected using the algorithm presented in Section 2 based on a single-point initialization within the vessel tree of interest. The output of this detection algorithm was then compared to markings made by an expert investigator. Note that the expert markings denote large areas that are likely to contain plaques while the proposed detection algorithm finds the outline of the detected plaques.

First, we show examples of plaque detection on 2D slices where the behavior of the algorithm is easy to visualize. Figures 4 and 5 show examples of non-calcified plaques that cause negative and positive remodeling of the vessel wall, respectively. Each figure shows the initial interior and exterior surfaces, both surfaces after evolution with the local means separation energy, the expert markings, and the detected plaque.

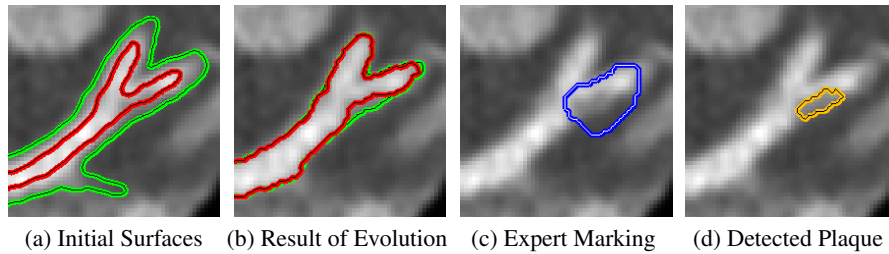


**Fig. 4.** A 2D view of detection results on the LAD (also shown in Figure 6a). The vessel demonstrates *negative* remodeling in the presence of plaque. The images depict (a) the initial interior and exterior surfaces, (b) the result of evolution with the local means separation energy, (c) the expert markings, and (d) the detected plaque.

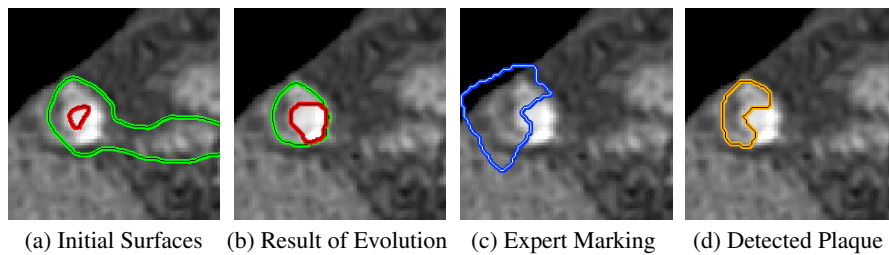


**Fig. 5.** A 2D view of detection results on the RCA (also shown in Figure 6d). The vessel demonstrates *positive* remodeling in the presence of plaque. The images depict (a) the initial interior and exterior surfaces, (b) the result of evolution with the local means separation energy, (c) the expert markings, and (d) the detected plaque.

Figure 6 shows rendered 3D views of the results from all 4 datasets that contained soft plaques. For each vessel tree, the segmented vessel is shown with truth markings and detected plaques. The datasets include plaques located in the LAD, LCX, and RCA vessel trees. In these experiments, plaques were identified well based on a single-click input. In total, 8 plaques were marked by the expert investigator within the 4 datasets. The proposed algorithm correctly identified 7 of 8 (87.5%) plaques with 1 false negative and 0 false positives. Additionally, the 4 datasets in which the LAD, LCX, and RCA were determined to be free of plaques were tested and, the algorithm correctly detected 0 plaques.

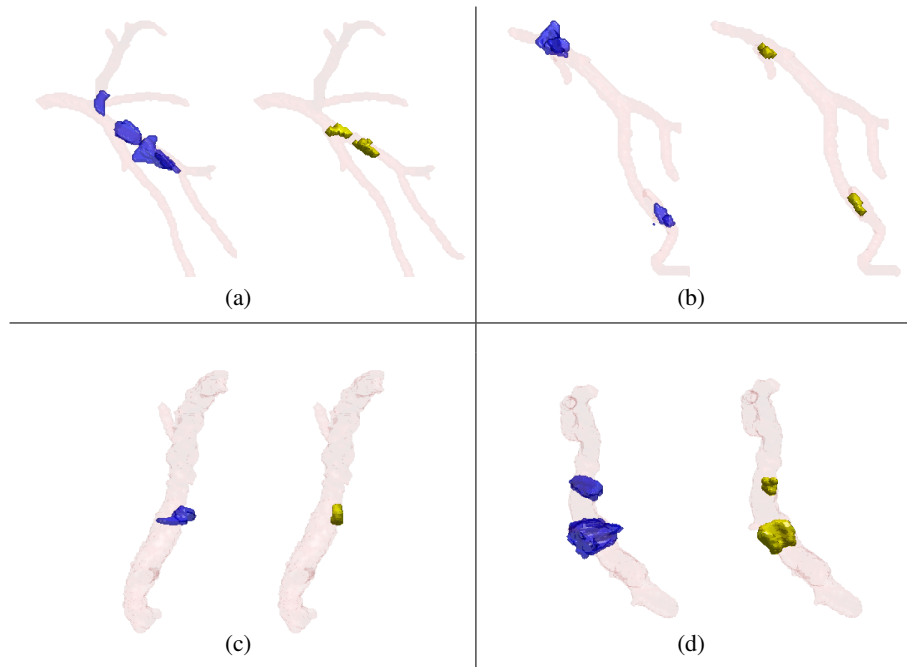


**Fig. 6.** 3D Renderings of detection results on the (a) LAD, (b) LCX, and (c, d) RCA. For each, the expert markings are shown in blue on the left, and the detection results are shown in yellow on the right.

## 4 Conclusions

In this note, we presented a technique that is capable of segmenting vessel trees and detecting non-calcified plaques automatically based on a very simple user input. The algorithm is based on a localized active contour framework that employs a scale parameter to restrict the statistical characteristics of the vessel into local regions. This allows simple probabilistic models based on local means to accurately extract the vessel and find areas where soft plaques exist. Experiments have shown good results that match experts' markings regarding the location of plaques.

Future work on this method will include coupling the evolution of the interior and exterior surfaces so that information about local intensities and geometries can be shared in order to detect plaques more robustly. Furthermore, a larger study is planned in which a larger number of datasets will be analyzed, a quantitative analysis will be performed, and the method will be compared with intravascular ultrasound imagery to confirm the presence and composition of detected plaques. We believe this work has the potential of being an important step forward in automatically detecting non-calcified plaques, which have been clearly linked with the occurrence of heart attacks and stroke.

## References

1. Schroeder, S., Kopp, A., Burgstahler, C.: Noninvasive plaque imaging using multislice detector spiral computed tomography. *Seminars in Thrombosis and Hemostasis* **33**(2) (2007) 203–209
2. Saur, S., Alkadhi, H., Desbiolles, L., Szekely, G., Cattin, P.: Automatic detection of calcified coronary plaques in computed tomography data sets. In: *Proceedings of Medical Imaging and Computing and Computer Assisted Intervention*. (2008) 170–177
3. Brunner, G., Kurkure, U., Chittajallu, D., Yalamanchili, R., Kakadiaris, I.: Toward unsupervised classification of calcified arterial lesions. In: *Proceedings of Medical Imaging and Computing and Computer Assisted Intervention*. (2008) 144–152
4. Achenbach, S., Moselewski, F., Ropers, D., Ferencik, M., Hoffmann, U., MacNeill, B., Pohle, K., Baum, U., Anders, K., Jang, I., Daniel, W.G., Brady, T.J.: Detection of Calcified and Noncalcified Coronary Atherosclerotic Plaque by Contrast-Enhanced, Submillimeter Multidetector Spiral Computed Tomography. *Circulation* **109**(1) (2004) 14–17
5. Pohle, K., Achenbach, S., MacNeill, B., Ropers, D., Ferencik, M., Moselewski, F., Hoffmann, U., Brady, T., Jang, I.K., Daniel, W.G.: Characterization of non-calcified coronary atherosclerotic plaque by multi-detector row CT: Comparison to IVUS. *Atherosclerosis* **190** (2007) 174–180
6. Virmani, R., Burke, A., Farb, A., Kolodgie, F.: Pathology of the vulnerable plaque. *Journal of the American College of Cardiology* **47**(8-C) (2006) 13–18
7. Renard, F., Yang, Y.: Image segmentation for detection of soft plaques in multidetector CT images. In: *Southwest Symposium on Image Analysis and Interpretation*. (2008) 121–124
8. Lankton, S., Tannenbaum, A.: Localizing region-based active contours. *IEEE Trans. on Image Processing* **17**(11) (Nov. 2008) 2029–2039
9. Sum, K., Cheung, P.: Vessel extraction under non-uniform illumination: A level set approach. *IEEE Trans. on Biomedical Engineering* **55**(1) (Jan. 2008) 358–360
10. Li, C., Kao, C.Y., Gore, J.C., Ding, Z.: Minimization of region-scalable fitting energy for image segmentation. *IEEE Trans. on Image Processing* **17**(10) (Oct. 2008) 1940–1949
11. Sethian, J.: *Level Set Methods and Fast Marching Methods*, Second Edition. Springer, New York, NY (1999)
12. Osher, S., Fedkiw, R.: *Level Set Methods and Dynamic Implicit Surfaces*. Cambridge University Press, New York, NY (2003)
13. Whitaker, R.T.: A level-set approach to 3D reconstruction from range data. *International Journal of Computer Vision* **29**(3) (1998) 203–231
14. Chan, T., Vese, L.: Active contours without edges. *IEEE Trans. on Image Processing* **10**(2) (February 2001) 266–277
15. A. Yezzi, J., Tsai, A., Willsky, A.: A fully global approach to image segmentation via coupled curve evolution equations. *Journal of Visual Communication and Image Representation* **13**(1) (March 2002) 195–216